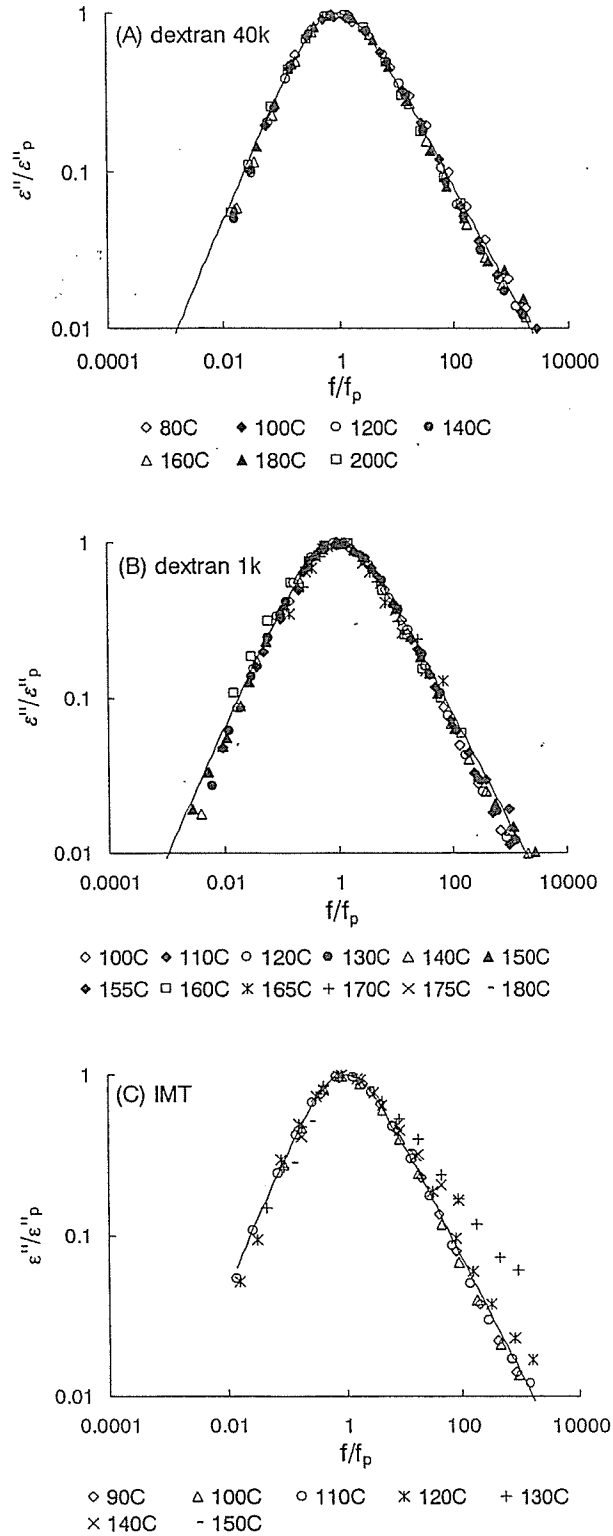

Figure 5. Normalized plot of imaginary permittivity for the Maxwell-Wagner–like process observed in freeze-dried dextran 40k (A), dextran 1k (B) and IMT (C) with a Teflon sheet inserted.

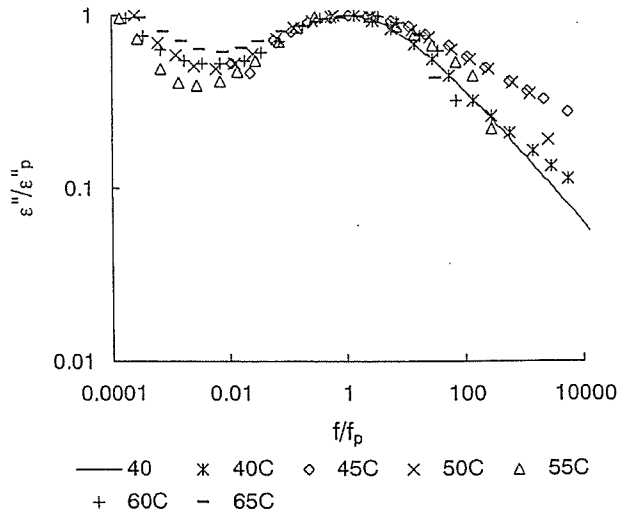

Figure 6. Normalized plot of imaginary permittivity for α-relaxation observed in freeze-dried α-glucose with a Teflon sheet inserted.

mechanism for this charge transfer process may be different from that for the proton-hopping–like process observed for IMT, dextran 1k, and dextran 40k. This was thought to be because this process occurred above T_g, whereas the proton-hopping–like process for IMT, dextran 1k, and dextran 40k occurred below T_g.

Temperature Dependence of Relaxation Time Determined by DES

Figure 7A shows the temperature dependence of the relaxation time of the proton-hopping–like process (τ_{DES}) observed for the freeze-dried dextran 40k, dextran 1k, and IMT, as well as that of the dielectric relaxation time of α-relaxation observed for the freeze-dried α-glucose. Figure 7A also shows the relaxation time of the molecular rearrangement motions in the freeze-dried α-glucose series, calculated from the observed T_g values according to the AGV (solid line) and VTF (dotted line) equations below and above T_g, respectively. The assumption that the fictive temperature (T_f) is equal to T_g (newly formed glass) and the fragility parameter (m) is equal to 70 was made, as reported for amorphous indomethacin.[26] The calculated relaxation time below T_g was not affected by varying the m value from 40 to 100, whereas that above T_g was largely dependent on the m value.[27]

The dielectric relaxation time observed for the freeze-dried α-glucose appeared to reach approximately 100 s at T_g, confirming that α-relaxation is

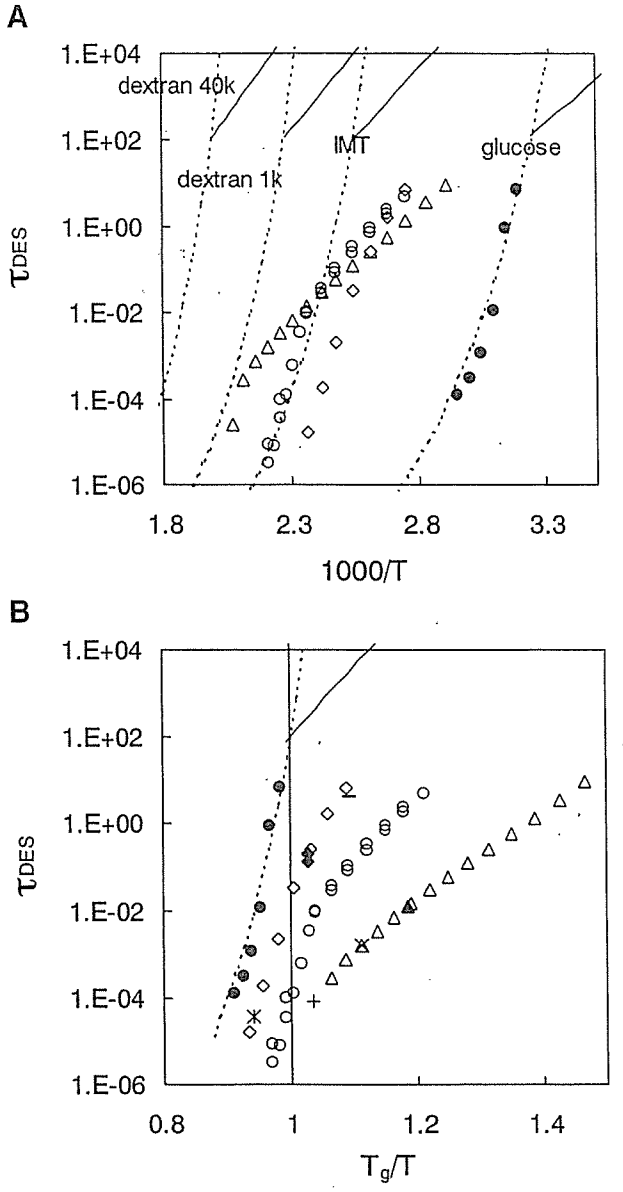

Figure 7. Relaxation time of the proton-hopping–like process observed in freeze-dried dextran 40k (△), dextran 1k (○) and IMT (◇), and that of α-relaxation observed in freeze-dried α-glucose (●) determined with dry samples at various temperatures, plotted against $1000/T$ (A) and T_g/T (B). Solid and dotted lines represent the relaxation time of molecular rearrangement motions calculated according to the AGV and VTF equations, respectively. (B) Also encloses the relaxation time determined with dextran 40k at 25°C and 43% RH (▲), 60% RH (×), and 75% RH (+), and that determined with IMT at 25°C and 23% RH (–), 43% RH (◆), and 60% RH (*).

responsible for this process. This is further supported by the finding that the observed dielectric relaxation time was almost coincident with the relaxation time of molecular rearrangement motions calculated using the VTF equation, although the relaxation time is only an approximation due to the assumed m value.

The τ_{DES} observed for the freeze-dried dextran 40k, dextran 1k, and IMT was shorter than the calculated relaxation time of molecular rearrangement motions (Fig. 7A), indicating that the proton-hopping–like process is faster than molecular rearrangement motions. A plot of the τ_{DES} versus the temperature scaled to T_g in order to conceal the effect of differing T_g values (Fig. 7B), was not in good agreement with the data obtained from different molecular weights. As molecular weight increased, the τ_{DES} at T_g decreased and the difference between the τ_{DES} and the relaxation time of molecular rearrangement motions increased. These results suggest that the rate of the proton-hopping–like process is determined not only by the molecular mobility indicated by the T_g value. If the observed quasi-dc process is assumed to be due to the proton-hopping–like process occurring in clusters constructed between hydroxy groups in the glucose unit as described above, the rate of the process may be affected by the cluster size and distance between clusters, which may depend on the molecular weight. Thus, the difference in molecular weight may result in a difference in the rate of proton-hopping–like process at T_g in addition to a difference in T_g values.

Figure 7B also shows the τ_{DES} observed for freeze-dried dextran 40k and IMT containing moisture. The temperature dependence of the τ_{DES} was not affected by the presence of moisture, and changes in the τ_{DES} were attributable only to changes in T_g. These findings suggest that moisture does not affect the rate of proton-hopping–like process itself, but enhances the process by increasing the molecular mobility as indicated by T_g.

As shown in Figure 7B, the slope of the τ_{DES} versus T_g/T plot increased as the temperature approached T_g from a lower temperature. These changes in temperature dependence were similar to those observed for the relaxation time of molecular rearrangement motions (line in Fig. 7). This similarity in the temperature dependence suggests that the proton-hopping–like process is linked to molecular rearrangement motions such that changes in the temperature dependence of the latter process around T_g result in changes in the

temperature dependence of the former process. Thus, enhancement of molecular rearrangement motions may enhance the proton-hopping–like process. The close relationship between the proton-hopping–like process and molecular rearrangement motions seems to be confirmed by the finding that enhancement in the proton-hopping–like process upon absorption of moisture can be explained only by the decrease in T_g, as described above.

Temperature Dependence of Correlation Time Determined by NMR Relaxation Measurement

Figure 8 shows the temperature dependence of the $T_{1\rho}$ measured for backbone carbon in the freeze-dried IMT. The $T_{1\rho}$ for backbone carbon in the freeze-dried dextran 40k reported previously[11] is also shown in the figure. $T_{1\rho}$ is plotted against $1/T$ in Figure 8A and against the temperature scaled to T_g in Figure 8B. Decreases in $T_{1\rho}$ with increasing temperature were observed for both freeze-dried IMT and dextran 40k even at temperatures below T_g. These shapes of temperature dependence suggest that $T_{1\rho}$ can detect the enhancement of molecular rearrangement motions associated with glass transition partially occurring even at temperatures below T_g.

Correlation time τ_c can be calculated from the observed $T_{1\rho}$ according to eq. (1) if the minimum value of $T_{1\rho}$ is known.[28]

$$\frac{1}{T_{1\rho}} = \frac{A\tau_c}{1 + 4\omega_1^2\tau_c^2} \qquad (1)$$

where ω_1 is the strength of spin-locking, and $\omega_1^2\tau_c^2$ is equal to 0.5 when $T_{1\rho}$ is the minimum. The change in $T_{1\rho}$ for the freeze-dried IMT equilibrated at 60% RH decreased at high temperatures, and $T_{1\rho}$ appeared to approach the minimum value. The value of A in eq. (1) was calculated assuming that the minimum value of $T_{1\rho}$ can be approximated from the smallest value of $T_{1\rho}$ measured at 60% RH, and used in the calculation of τ_c. Because $T_{1\rho}$ minimum was not observed for freeze-dried dextran 40k even at 75% RH, the value of A for freeze-dried dextran 40k was calculated from the minimum value of $T_{1\rho}$ measured at 86% RH, which had been reported previously.[11] The τ_c value calculated for dextran 40k and IMT is plotted against the temperature scaled to T_g in Figure 9A, and compared with the relaxation time of the proton-hopping–like process (τ_{DES}) in Figure 9B. The relaxation time of molecular rearrangement motions determined

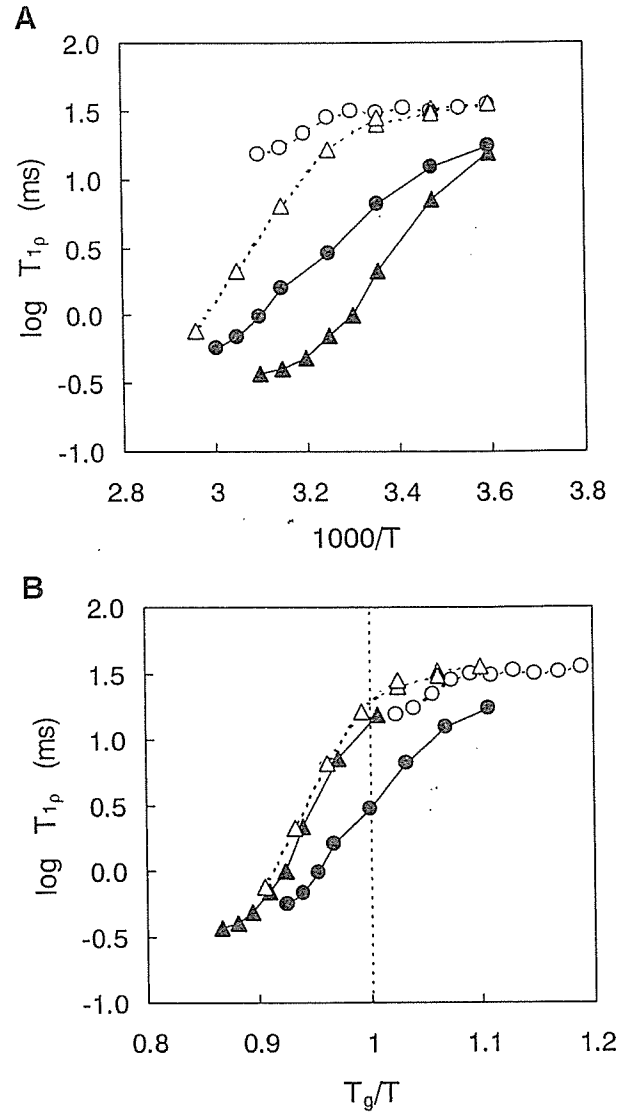

Figure 8. $T_{1\rho}$ of freeze-dried IMT equilibrated at 43% RH (△) and 60% RH (▲), plotted against $1000/T$ (A) and T_g/T (B). $T_{1\rho}$ of freeze-dried dextran 40k at 60% RH (○) and 75% RH (●) reported previously[11] is shown.

calorimetrically is also shown in Figure 9B. The τ_c value derived from $T_{1\rho}$ was shorter than the relaxation time of molecular rearrangement motions for both freeze-dried IMT and dextran 40k.

The $T_{1\rho}$-derived τ_c for the freeze-dried IMT and dextran 40k was on nearly the same order as the τ_{DES} around a T_g/T of 0.95 and 1.06, respectively, and was much smaller than the relaxation time of molecular rearrangement motions determined calorimetrically. As the T_g/T increased above 0.95 and 1.06, the $T_{1\rho}$-derived τ_c for the freeze-dried IMT and dextran 40k, respectively, diverged significantly from the plots for the τ_{DES}. A similar

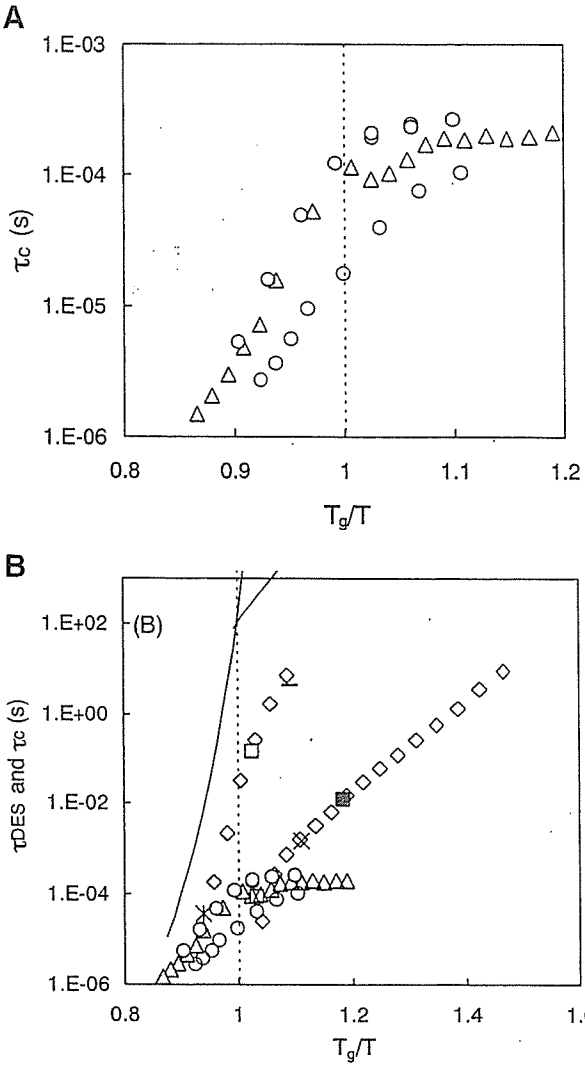

Figure 9. (A) τ_c for the methine carbon of dextran 40k at 60% RH (△), dextran 40k at 75% RH (○), IMT at 43% RH (○), and IMT at 60% RH (△) calculated from the observed value of $T_{1\rho}$. (B) Comparison of the τ_c of methine carbon with the τ_{DES} of the proton-hopping–like process for dextran 40k (◇) and IMT (◇) determined with dry samples at various temperatures, as well as τ_{DES} determined for dextran 40k at 25°C and 43% RH (▩), 60% RH (×), 75% RH (+), and τ_{DES} determined for IMT at 25°C and 23% RH (−), 43% RH (□), and 60% RH (∗). The relaxation time of molecular rearrangement motion determined calorimetrically (solid line) is also shown.

divergence of $T_{1\rho}$-derived τ_c from a DES correlation time at temperatures below T_g has been reported for glucose.[15]

To elucidate the reason for the divergence of the $T_{1\rho}$-derived τ_c from the plots for the τ_{DES}, the τ_{DES} value determined from the dielectric spectrum

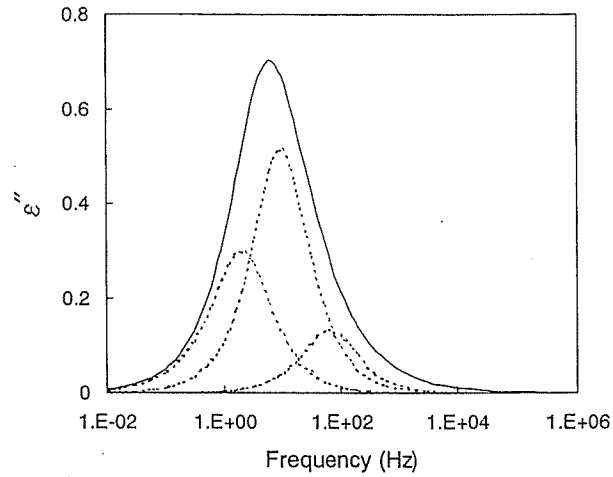

Figure 10. Dielectric relaxation spectrum of freeze-dried IMT at 120°C (solid line). Dashed lines represent three components of the Debye relaxation used for the transformation of τ_{DES} to $T_{1\rho}$.

reflecting the proton-hopping–like process was transformed to the corresponding $T_{1\rho}$ value and compared with the experimentally determined $T_{1\rho}$. The dielectric spectrum obtained for the freeze-dried IMT was first divided into three components of the Debye relaxation, and the three sets of τ and its fraction (f) were then calculated according to eq. (2).[29] An example of the imaginary permittivity (ε'') versus frequency plots used for the analysis is shown in Figure 10.

$$\varepsilon'' = \sum_{i=1}^{3} \frac{\Delta\varepsilon_i \omega \tau_i}{1 + \omega^2 \tau_i^2} \qquad (2)$$

$$\text{where } \Delta\varepsilon_i = f_i(\Delta\varepsilon_1 + \Delta\varepsilon_2 + \Delta\varepsilon_3)$$

The three sets of τ and f obtained were used to calculate the spectral density $J(\omega)$ according to eq. (3).[28]

$$J(\omega) = \sum_{i=1}^{3} \frac{f_i \tau_i}{1 + 4\omega^2 \tau_i^2} \qquad (3)$$

Calculated $J(\omega)$ at temperatures ranging from 90° to 150°C are shown as a function of frequency in Figure 11A. Figure 11B shows the temperature dependence of J at 57 kHz, which corresponds to the ω value of the NMR instrument used in this investigation. The value of $T_{1\rho}$ corresponding to the τ_{DES} was calculated from the obtained J according to eq. (4),[28] and the result is shown in Figure 12A.

$$\frac{1}{T_{1\rho}} = AJ = \frac{1 + 4\omega_1^2 \tau_c^2}{T_{1\rho(\min)} \tau_c} J \qquad (4)$$

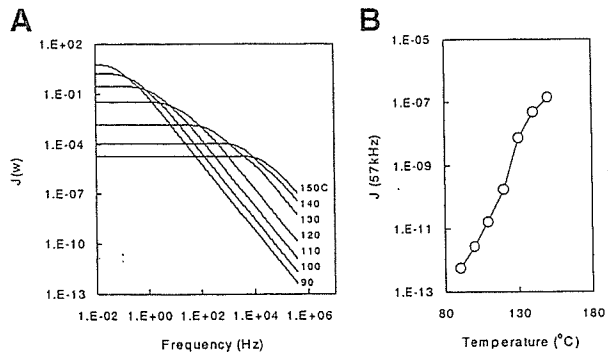

Figure 11. Spectral density calculated from dielectric relaxation spectrum of freeze-dried IMT as a function of frequency (A) and at 57 kHz as a function of temperature (B).

where $\omega^2\tau_c^2$ was assumed to be equal to 0.5. The $T_{1\rho}$ value corresponding to the τ_{DES} for the freeze-dried dextran 40k was calculated from the dielectric spectrum in a similar manner as that of IMT. However, the dielectric spectrum was divided into two rather than three components, because the distribution of the spectrum for dextran 40k was smaller than that for IMT. The value of $T_{1\rho}$ calculated from dielectric spectrum (DES-derived $T_{1\rho}$) is shown in Figure 12B.

Figure 12 encloses the experimentally determined $T_{1\rho}$ value compared with the DES-derived $T_{1\rho}$ value. The measured $T_{1\rho}$ was close to the DES-derived $T_{1\rho}$ around a T_g/T of 0.95 and 1.06 for freeze-dried IMT and dextran 40k, respectively. However, as the T_g/T increased above these values, the measured $T_{1\rho}$ diverged from the DES-derived $T_{1\rho}$ and approached a plateau on the order of 10 ms. This plateau for the measured $T_{1\rho}$ is thought to be due to static spin–spin interactions that affect $T_{1\rho}$. Namely, $T_{1\rho}$ is determined predominantly by static factors rather than by molecular mobility at lower temperatures,[30] at which molecular mobility is very low. As temperature increases above a certain point, the contribution of molecular mobility to $T_{1\rho}$ increases to a degree comparable to static spin–spin interactions, and begins to decrease the measured value of $T_{1\rho}$. The critical temperature at which the increase in molecular mobility begins to be reflected in $T_{1\rho}$ is considered to be the T_{mc} defined previously as the T_g determined by the NMR relaxation time.[9] For freeze-dried dextran 40k, the T_g/T value of 1.06 was close to that of 1.07 calculated for a sample with a T_g of 58°C and a T_{mc} of 35°C (60% RH), and to that of 1.05 calculated for a sample with a T_g of 35°C and a T_{mc} of 20°C

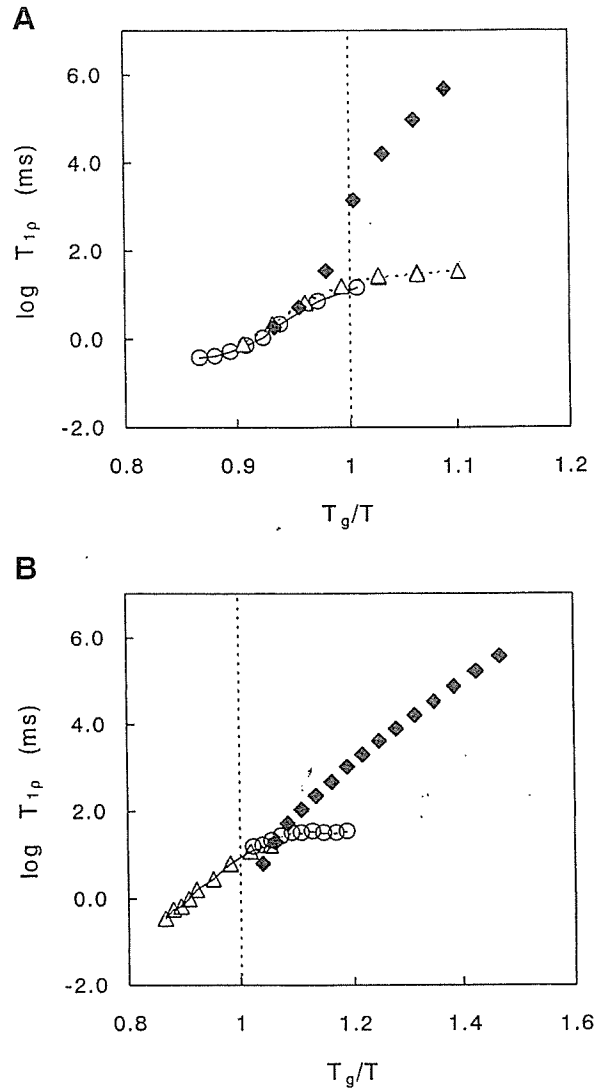

Figure 12. $T_{1\rho}$ observed at 43% RH (△) and 60% RH (○) for freeze-dried IMT (A) and that at 60% RH (○) and 75% RH (△) for freeze-dried dextran 40k (B), compared with $T_{1\rho}$ estimated based on the spectral density calculated from dielectric spectrum (◆).

(75% RH). These findings suggest that $T_{1\rho}$ cannot reflect molecular mobility at temperatures below T_{mc}.

In contrast to the freeze-dried dextran 40k, freeze-dried IMT exhibited a DES-derived $T_{1\rho}$ much larger than the measured $T_{1\rho}$ even at temperatures around T_g, at which $T_{1\rho}$ is expected to reflect molecular mobility. This difference between IMT and dextran 40k suggests that a decrease in molecular weight decreases the rate of the proton-hopping–like process. Thus, even at T_g, the timescale of the proton-hopping–like process

in freeze-dried IMT may become on the order larger than 10 ms, at which $T_{1\rho}$ cannot reflect the rate of process.

Molecular motions in freeze-dried IMT and dextran 40k were too slow to be reflected in $T_{1\rho}$ at temperatures well below T_g such that the measured $T_{1\rho}$ diverged significantly from the DES-derived $T_{1\rho}$ (Fig. 12). However, the coincidence of the measured $T_{1\rho}$ and the DES-derived $T_{1\rho}$ around a T_g/T of 0.95 and 1.06 (although the range is very small) suggests that the timescale of molecular motion reflected in $T_{1\rho}$ is on the same order as that of the proton-hopping–like process. As shown in Figure 7, the τ_{DES} decreased rapidly as temperature approached T_g, showing a similar shape of temperature dependence to that of molecular rearrangement motions. The $T_{1\rho}$-derived τ_c also showed a similar shape of temperature dependence (Fig. 9). The similarity of the temperature-dependence patterns suggests that the molecular motions reflected in $T_{1\rho}$ are linked to molecular rearrangement motions, such that enhancement of molecular rearrangement motions enhances the molecular motions reflected in $T_{1\rho}$. Such linkage was also observed between molecular rearrangement motions and molecular motion reflected in τ_{DES}, as described above (Fig. 7). Fujiwara and Nagayama[31] reported that the exact correlation functions expressed by multiexponential decay observed in the NMR relaxation of macromolecules were well approximated by a single exponential decay. This seems to support the interpretation that molecular rearrangement motions are linked to the molecular motions reflected in $T_{1\rho}$ and τ_{DES}. Because of this linkage between molecular motions, changes in the temperature dependence of molecular rearrangement motions related to the instability of amorphous formulations may be detected by measurement of $T_{1\rho}$ and τ_{DES}.

$T_{1\rho}$ of ^{13}C in the polymer backbone was used as a measure of molecular mobility in the present investigation. However, previous investigations have demonstrated that changes in the temperature dependence for molecular rearrangement motions of freeze-dried dextran can be detected by the T_1 of ^{13}C in the polymer backbone,[10] as well as the T_1 and $T_{1\rho}$ of ^1H.[11] Figure 13 compares the temperature dependence of $T_{1\rho}$ of ^{13}C in the dextran backbone described in this article with those of T_1 of ^{13}C, and T_1 and $T_{1\rho}$ of ^1H reported previously. A change in the slope of the NMR relaxation time versus $1/T$ plot was clearly shown around T_{mc} indicated by arrows. Thus, the shape of

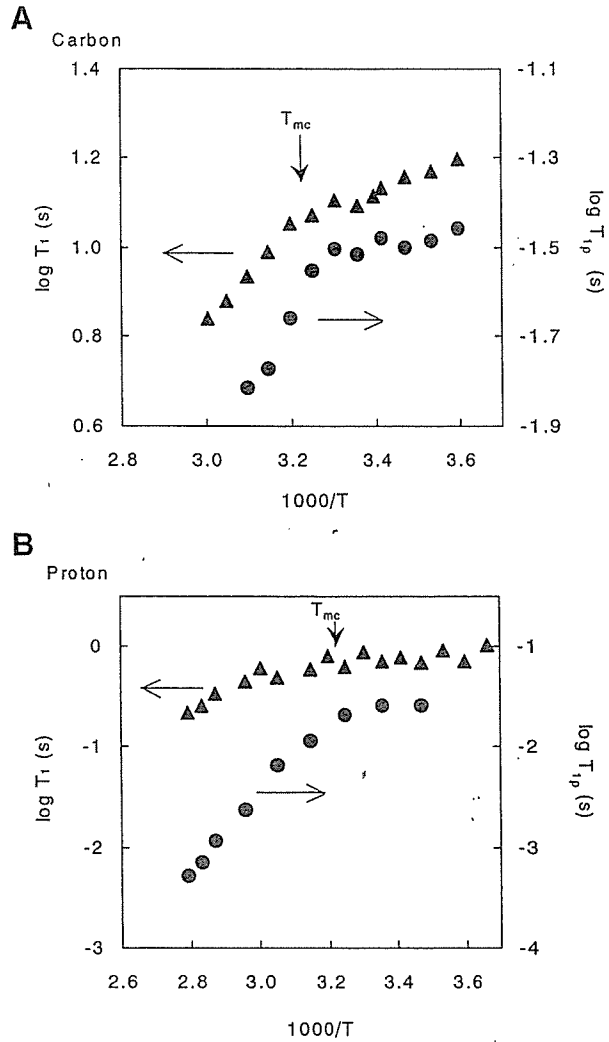

Figure 13. Temperature dependence of T_1 (▲) and $T_{1\rho}$ (●) of methine carbon (A) and proton (B) in the freeze-dried dextran 40k observed at 60% RH.

temperature dependence of T_1, which reflects a smaller timescale of molecular motions than $T_{1\rho}$, was similar to that of $T_{1\rho}$. This finding suggests that molecular motion with a smaller timescale than the molecular motion reflected in $T_{1\rho}$ is also linked to molecular rearrangement motions.

CONCLUSIONS

DES was able to detect molecular rearrangement motions in freeze-dried α-glucose. However, molecular rearrangement motions in freeze-dried dextran 40k, dextran 1k, and IMT were too slow to be observed by DES from 0.01 Hz to 100 kHz,

and proton-hopping–like process rather than molecular rearrangement motions was reflected in the dielectric spectra. The τ_c for the backbone carbon of dextran 40k and IMT, calculated from the observed $T_{1\rho}$ value, was found to be close to the relaxation time of proton-hopping–like process (τ_{DES}) at temperatures around T_g. The timescales for molecular motions reflected in the τ_c and τ_{DES} were significantly smaller than that for molecular rearrangement motions, but the shapes of temperature dependence for the τ_c and τ_{DES} were similar to that of the relaxation time of molecular rearrangement motions. This suggests that molecular motions reflected in the τ_{DES} and the τ_c are linked to molecular rearrangement motions. Because of this linkage between molecular motions, changes in the temperature dependence of molecular rearrangement motions related to the instability of amorphous formulations may be detected by measurement of $T_{1\rho}$ and τ_{DES}.

This thought seems to address the question why changes in molecular rearrangement motions with a relaxation time longer than 100 s at sub-T_g can be detected by measuring NMR relaxation times that reflect molecular motions on the order of 10 kHz and 1 MHz.

REFERENCES

1. Shamblin SL, Tang X, Chang L, Hancock BC, Pikal MJ. 1999. Characterization of the time scales of molecular motion in pharmaceutically important glasses. J Phys Chem 103:4113–4121.
2. Yoshioka S, Aso Y, Kojima S. 2000. Temperature dependence of bimolecular reactions associated with molecular mobility in lyophilized formulations. Pharm Res 17:925–929.
3. Yoshioka S, Aso Y, Kojima S. 2004. Temperature- and glass transition temperature-dependence of bimolecular reaction rates in lyophilized formulations described by the Adam-Gibbs-Vogel equation. J Pharm Sci 93:1062–1069.
4. Aso Y, Yoshioka S, Kojima S. 2004. Molecular mobility-based prediction of the crystallization rate of amorphous nifedipine and phenobarbital in PVP solid dispersions. J Pharm Sci 93:384–391.
5. Yoshioka S, Aso Y, Nakai Y, Kojima S. 1998. Effect of high molecular mobility of poly(vinyl alcohol) on protein stability of lyophilized γ-globulin formulations. J Pharm Sci 87:147–151.
6. Yoshioka S, Tajima S, Aso Y, Kojima S. 2003. Inactivation and aggregation of β-galactosidase in lyophilized formulation described by Kohlrausch-Williams-Watts stretched exponential function. Pharm Res 20:1655–1660.
7. Kalichevsky MT, Jaroszkiewicz EM, Ablett S, Blanshard JMV, Lillford PJ. 1992. The glass transition of amylopectin measured by DSC, DMTA and NMR. Carbohydr Polym 18:77–88.
8. Kalichevsky MT, Jaroszkiewicz EM, Blanshard JMV. 1993. A study of the glass transition of amylopectin-sugar mixtures. Polymer 34:346–358.
9. Yoshioka S, Aso Y, Kojima S. 1999. The Effect of excipients on the molecular mobility of lyophilized formulations, as measured by glass transition temperature and NMR relaxation-based critical mobility temperature. Pharm Res 16:135–140.
10. Yoshioka S, Aso Y, Kojima S, Sakurai S, Fujiwara T, Akutsu H. 1999. Molecular mobility of protein in lyophilized formulations linked to the molecular mobility of polymer excipients, as determined by high resolution ^{13}C solid-state NMR. Pharm Res 16:1621–1625.
11. Yoshioka S, Aso Y, Kojima S. 2002. Different molecular motions in lyophilized protein formulations as determined by laboratory and rotating frame spin-lattice relaxation times. J Pharm Sci 91:2203–2210.
12. Yoshioka S, Aso Y, Kojima S. 2003. Mobility of lyophilized poly(vinylpyrrolidone) and methylcellulose as determined by the laboratory and rotating frame spin-lattice relaxation times of ^{1}H and ^{13}C. Chem Pharm Bull 51:1289–1292.
13. Andronis V, Zografi G. 1998. The molecular mobility of supercooled amorphous indomethacin as a function of temperature and relative humidity. Pharm Res 15:835–842.
14. Noel TR, Parker R, Ring SG. 2000. Effect of molecular structure and water content on the dielectric relaxation behaviour of amorphous low molecular weight carbohydrates above and below their glass transition. Carbohydr Res 329:839–845.
15. Moran GR, Jeffrey KR, Thomas JM, Stevens JR. 2000. A dielectric analysis of liquid and glassy solid glucose/water solutions. Carbohydr Res 328: 573–584.
16. Montes H, Cavaille JY. 1999. Secondary dielectric relaxations in dried amorphous cellulose and dextran. Polymer 40:2649–2657.
17. Derbyshire H, Feldman Y, Bland CR, Broadhead J, Smith G. 2002. A study of the molecular properties of water in hydrated mannitol. J Pharm Sci 91: 1080–1088.
18. Suherman PM, Taylor PM, Smith G. 2002. Development of a remote electrode system for monitoring the water content of materials inside a glass vial. Pharm Res 19:337–344.
19. Jain SK, Johari GP. 1988. Dielectric studies of molecular motions in the glassy states of pure and aqueous poly(vinylpyrrolidone). J Phys Chem 92: 5851–5854.

20. Duddu SP, Sokoloski TD. 1995. Dielectric analysis in the characterization of amorphous pharmaceutical solids. 1. Molecular mobility in poly(vinylpyrrolidone)-water systems in the glassy state. J Pharm Sci 84:773–776.
21. Barker SA, He R, Craig DQM. 2001. Low frequency dielectric investigations into the relaxation behavior of frozen polyvinylpyrrolidone-water systems. J Pharm Sci 90:157–164.
22. Yoshioka S, Aso Y, Otsuka T, Kojima S. 1995. Water mobility in poly(ethylene glycol)-, poly(vinylpyrrolidone)-, and gelatin-water systems, as indicated by dielectric relaxation time, spin-lattice relaxation time, and water activity. J Pharm Sci 84:1072–1077.
23. Jonscher AK. 1991. Low-frequency dispersion in volume and interfacial situations. J Mater Sci 26:1618–1626.
24. Bone S, Eden J, Gascoyne PRC, Pethig R. 1981. Conduction and dielectric polarization in proteins and molecular complexes. J Chem Soc Faraday Trans 1 77:1729–1732.
25. Careri G, Geraci M, Giansanti A, Rupley JA. 1985. Protonic conductivity of hydrated lysozyme powders at megahertz frequencies. Proc Natl Acad Sci USA 82:5342–5346.
26. Crowley KJ, Zografi G. 2001. The use of thermal methods for predicting glass-former fragility. Thermochim Acta 380:79–93.
27. Boehmer R, Ngai KL, Angell CA, Plazek DJ. 1993. Nonexponential relaxations in strong and fragile glass formers. J Chem Phys 99:4201–4209.
28. Farrar TC, Becker ED. 1971. Pulse and Fourier transform NMR: Introduction to theory and methods. New York: Academic Press.
29. Wada H. 1987. Koubunshi no denkibussei. Tokyo: Shokabo Publishing.
30. Schaefer J, Stejskal EO, Steger TR, Sefcik MD, McKay RA. 1980. Carbon-13 $T_{1\rho}$ experiments on solid glassy polymers. Macromolecules 13:1121–1126.
31. Fujiwara T, Nagayama K. 1985. The wobbling-in-a-cone analysis of internal motion in macromolecules. J Chem Phys 83:3110–3117.

Available online at www.sciencedirect.com
SCIENCE DIRECT®
International Journal of Pharmaceutics 300 (2005) 38–47
international journal of pharmaceutics
www.elsevier.com/locate/ijpharm

Cholesteryl hemisuccinate as a membrane stabilizer in dipalmitoylphosphatidylcholine liposomes containing saikosaponin-d

Wu-xiao Ding[a], Xian-rong Qi[a,*], Ping Li[b], Yoshie Maitani[c], Tsuneji Nagai[c]

[a] *Department of Pharmaceutics, School of Pharmaceutical Sciences, Peking University, Beijing 100083, China*
[b] *Department of Materia Medica and Pharmacology, China–Japan Friendship Hospital, Beijing 100029, China*
[c] *Institute of Medicinal Chemistry, Hoshi University, Shinagawa-Ku, Tokyo 142-8501, Japan*

Received 25 February 2005; received in revised form 12 April 2005; accepted 10 May 2005
Available online 22 June 2005

Abstract

In the present study, cholesteryl hemisuccinate (CHEMS) was evaluated for use as a membrane stabilizer in dipalmitoylphosphatidylcholine (DPPC) liposomes. Differential scanning calorimetry (DSC) and a calcein release study showed that CHEMS was more effective than cholesterol (CHOL) in increasing DPPC membrane stability. The findings of Fourier transform infrared spectroscopy (FT-IR) also suggested that CHEMS interacts with DPPC via both hydrogen bonding and electrostatic interaction. More importantly, CHEMS did not interact with saikosaponin-d (SSD), a triterpene saponin from Bupleurum species, unlike CHOL. SSD-containing liposomes with DPPC, CHEMS and DSPE-PEG could greatly decrease the hemolytic activity of SSD. This study demonstrated that CHEMS has more stabilization ability than CHOL since CHEMS may exhibit both hydrogen bond interaction and electrostatic interaction with DPPC membrane while CHOL only has hydrogen bond interaction, resulting in stable and low-hemolytic SSD-liposomes.

Keywords: Cholesteryl hemisuccinate; Saikosaponin-d; Saponin; Liposome; Differential scanning calorimetry; Fourier transform infrared spectroscopy

1. Introduction

Saikosaponin-d (SSD) (Fig. 1A), a triterpene saponin from Bupleurum species, has shown corticosterone-like activity (Yokoyama et al., 1984), Na^+-, K^+-ATPase inhibiting action (Zhou et al., 1996), immunoregulatory action (Ushio and Abe, 1991) and anti-platelet activating factor activity (Nakamura et al.,

Abbreviations: DPPC, dipalmitoylphosphatidylcholine; CHEMS, cholesteryl hemisuccinate; CHOL, cholesterol; SSD, saikosaponin-d; DSPE-PEG, methoxypolyethyeneglycol (Mr2000)-distearoylphosphatidylethanolamine; DSC, differential scanning calorimetry; FT-IR, Fourier transform infrared spectroscopy

* Corresponding author. Tel.: +86 10 82801584; fax: +86 10 82802791.
E-mail address: qixr2001@yahoo.com.cn (X.-r. Qi).

0378-5173/$ – see front matter © 2005 Elsevier B.V. All rights reserved.
doi:10.1016/j.ijpharm.2005.05.005

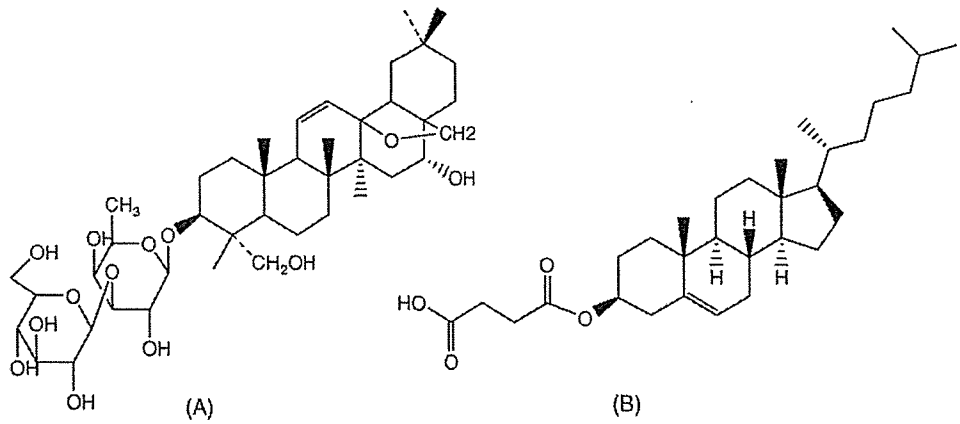

Fig. 1. Structures of saikosaponin-d (A) and cholesteryl hemisuccinate (B).

1993). It has been widely studied as a potential medication in the treatment of nephritis, nephrosis syndrome (Abe et al., 1986) and hepatic fibrosis (Cheng et al., 1999). Furthermore, bupleurum soup and particles for oral administration, the main active constituent of which is SSD, have achieved great success in the treatment of chronic glomerulonephritis and glomerulosclerosis (Zhang, 1993; Cheng, 1994).

SSD and other saikosaponins given in oral dosage form are not readily absorbed in the gastrointestinal tract and easily metabolized by glycosidase to less potent prosaikogenins before absorption occurs (Kida et al., 1998), leading to a dose of 200–300 mg and the need for treatment three times per day for adults. Therefore, the low level (less than 0.01%) of saikosaponins in Bupleurum species and their tendency to transform during separation and purification (Wen, 1993) hinder practical application in the clinic.

Other routes such as intraperitoneal and intramuscular administration have also been explored and are thought to enhance the corticosterone level in serum (Yokoyama et al., 1984; Zhong et al., 1993), however the risk of hemolysis should also be carefully considered. It is widely recognized that the hemolytic activity of SSD is caused by its complex with cholesterol (CHOL) on erythrocyte membrane, leading to membrane disruption and cell lysis. Driven by the need to reduce the hemolytic activity and make possible injections with less SSD, the liposome was chosen as a carrier for the present research because of its non-toxic, enhanced therapeutic efficacy and reduction of drug toxicity (Gregoriads, 1988).

It has been mentioned (Wang, 1992) that sterols with C_3-β-OH (including CHOL) form an insoluble complex with SSD, but, sterols with C_3-α-OH and esterified or glycosidated at C_3-OH do not. It is difficult to prepare liposomes containing SSD (SSD-liposomes), since SSD will form an insoluble complex with CHOL, which is routinely used to stabilize liposomes. Therefore, there is a great need for other membrane stabilizers for the preparation of SSD-liposomes.

Cholesteryl hemisuccinate (CHEMS) (Fig. 1B) is a CHOL-derivative esterified to the 3-hydroxyl group of CHOL and is supposed not to form a complex with SSD. Until now, no toxicity profiles about CHEMS have been reported. On the other hand, it has been found to increase specific immunogenicity of tumor cells by pretreating tumor cells with CHEMS (Skornick et al., 1986). And also, CHEMS was thought to protect against acetaminophen-induced hepatocellular apoptosis (Ray et al., 1996) and carbon tetrachloride-induced hepatotoxicity. It was proved to be a powerful cytoprotective agent against carbon tetrachloride hepatotoxicity in vivo (Fariss et al., 1993). CHEMS can form pH-sensitive fusogenic vesicles when incorporated into phosphatidylethanolamine bilayers and the pH is lowered to 5.5, resulting in H-II phase formation (Ismail et al., 2000; Se'rgio et al., 2004). CHEMS has also been demonstrated to alter acyl chain motion or fluidity in cell membranes (Dumas et al., 1997; Lai et al., 1985). It was proved by fluorescence polarization to be equally effective as CHOL in reducing the acyl chain mobility of DPPC above the phase transition temperature (Massey, 1998) and reported

to be a membrane stabilizer (Zhang et al., 2000). All these attributes contribute to the suitability of CHEMS as a membrane stabilizer in the preparation of SSD-liposomes, which has not been studied in the past.

The mechanism by which CHEMS acts as a membrane stabilizer is not fully understood and little research has been done on drug-loaded liposomes using CHEMS as a membrane stabilizer. Therefore, in the present study, CHEMS was investigated for its membrane stabilization ability using DSC, calcein release and FT-IR measurements. Furthermore, the hemolytic activity of SSD-liposomes using CHEMS as a unique membrane stabilizer was evaluated.

2. Materials and methods

2.1. Materials

Dipalmitoylphosphatidylcholine (DPPC), CHOL, succinic anhydride and methoxypolyethyeneglycol (Mr 2000)-distearoylphosphatidylethanolamine (DSPE-PEG) were purchased from NOF Corporation (Japan). Saikosaponin-d (SSD, purity of 95%) was extracted from the root of *Bupleurum falcatum* by the Department of Materia Medica and Pharmacology, China–Japan Friendship Hospital. A Dialysis membrane (cutoff 8000–14,000) was purchased from Membrane Filtration Products (San Antonio, USA). All other chemicals were of reagent grade.

2.2. Synthesis of CHEMS

CHEMS was prepared according to Kuhn et al. (1975), but with 4-dimethylaminopyridine (DMAP) added as a catalyzer. The molecular weight of CHEMS determined by ESI-TOF-MS was 486.74.

2.3. DSC analysis

Liposome suspensions containing DPPC and different amounts of CHOL, CHEMS and SSD were prepared with 1/10 PBS (pH 7.4) by the film hydration and bath sonication method, with a DPPC concentration of 100 mg/ml. Ten microliters of each liposome suspension (1 mg DPPC) was transferred into a 20-μl DSC aluminum pan and subjected to DSC analysis using a DSC 2010 (Thermal Analysis, Newcastle, USA). The scan rate employed was 0.5 °C/min over the temperature range 20–50 °C, and the reference pan was filled with 1/10 PBS. The transition enthalpies (ΔH, J/g of DPPC) were calculated from the peak areas using the integration program of the TA processor, within an experimental error of ±5%.

2.4. Calcein release study

Calcein-encapsulated liposomes (DPPC-, DPPC/CHOL (10:4)-, DPPC/CHEMS (10:4)-liposomes) were prepared by the reverse phase evaporation vesicle method (Szoka and Papahadjopoulos, 1978). Briefly, 25 mg of DPPC and specific amount of CHEMS or CHOL were dissolved in 15 ml of chloroform/isopropyl ether (2:1, v/v) and mixed with 5 ml of calcein solution (1×10^{-3} mol/l in 1/10 PBS). The mixtures were sonicated by probe sonicator to give a homogeneous emulsion and then placed on a vacuum rotary evaporator until the formation of liposome suspension. The liposomes were then extruded through 200 nm-pore sized polycarbonate film at 45 °C for two times and free calcein was separated by Sephadex G-100. Calcein release from the liposomes was carried out with a dialysis method both in 1/10 PBS and in 30% rabbit plasma at 37 ± 0.5 °C.

2.5. FT-IR analysis

DPPC mixtures with CHOL, CHEMS and SSD (all with a 1:1 molar ratio) were dissolved in chloroform or a chloroform–methanol mixture for SSD. The solvent was evaporated under vacuum, the dried lipid mixture was pressed into thin KBr tablets. The tablets were scanned on a Nicolet 5DX (Thermo Electron Corp., Waltham, USA) from 400 to 4000 cm^{-1}. The separate FT-IR spectrograms were combined over the region between 1800 and 1200 cm^{-1}, which contained the band position of the P=O stretching vibration (V_s P=O), the P=O asymmetric stretching vibration (V_{as} P=O) and the asymmetry flexual vibration of the quaternary ammonium of DPPC.

2.6. Turbidity measurement

Blank liposomes (DPPC/CHOL (10:4)- and DPPC/CHEMS (10:4)-liposomes) were prepared by the film hydration and probe sonication method to

give small unilammelar vesicles (SUVs, average size, 134.6 and 102.9 nm, respectively), with the DPPC concentration at 0.5 mg/ml. An equal volume of SSD suspension of 200 μg/ml or distilled water was added to the liposome suspension, and the relative turbidity ($A_t/A_0 \times 100\%$) of liposomes was measured at 550 nm at room temperature, where A_t and A_0 represent the absorption value at time t and 0 min at 550 nm, respectively.

2.7. Hemolytic activity

SSD-liposomes with serial concentrations of SSD were prepared with DPPC, CHEMS and/or DSPE-PEG by film hydration and probe sonication. A 0.3 ml volume of SSD solution or SSD-liposomes suspension (with a lipid concentration of 2.5 mg/ml and size of about 150 nm) was put into a 5 ml glass tube, and then 2.2 ml of saline and 2.5 ml of 2% rabbit erythrocyte suspension were added. The mixtures were incubated at 37 ± 0.5 °C for 3 h and then centrifuged at 2500 rpm for 10 min. The absorption value of the supernatant was measured at 540 nm by subtracting the blank.

3. Results

3.1. Effect of CHOL, CHEMS and SSD on DPPC membrane by DSC

As illustrated in Fig. 2 and Table 1, the maximal transition temperature from gel to liquid-crystalline (T_m) and the transition enthalpy (ΔH) of the DPPC bilayer was 39.52 °C and 24.24 J/g of DPPC, respectively, addition of CHOL and CHEMS decreased the T_m value slightly and the ΔH value markedly. The T_m values of the five formulations remained at about

Table 1
The maximal transition temperature from gel to liquid-crystalline (T_m) and ΔH value of DPPC liposomes with CHOL, CHEMS and SSD (each sample contained 1 mg DPPC)

Composition (molar ratio)	T_m (°C)	ΔH (J/g of DPPC)
DPPC	39.52	24.24
DPPC:CHOL (10:2)	39.28	5.26
DPPC:CHEMS (10:2)	38.28	1.162
DPPC:CHEMS (10:1)	39.34	11.89
DPPC:SSD (10:2)	38.68	23.54

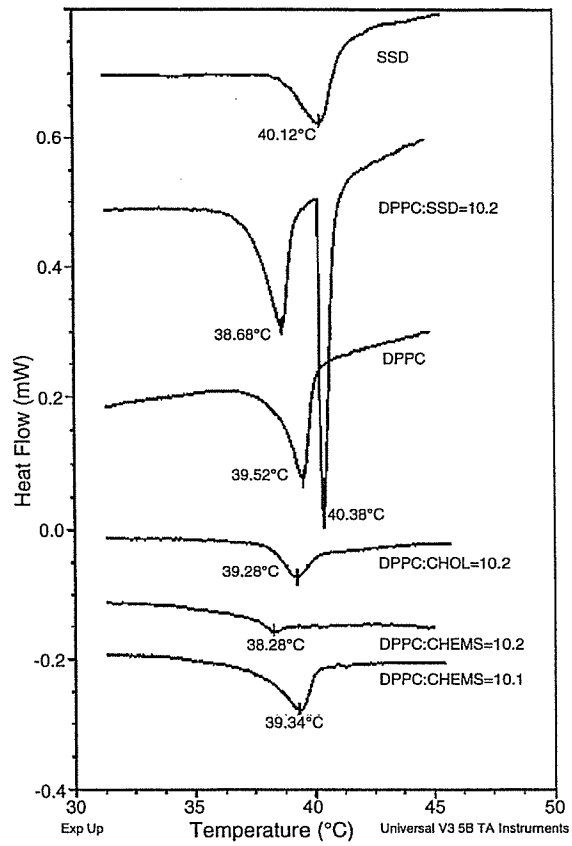

Fig. 2. DSC spectrograms of DPPC liposomes with CHEMS, CHOL and SSD.

39 °C, while the ΔH values of DPPC/CHOL (10:2)-, DPPC/CHEMS (10:1)- and DPPC/CHEMS (10:2)-liposomes were decreased markedly to 5.26, 11.89 and 1.162 J/g of DPPC, respectively.

We have found that a maximum amount of SSD that can retain in the lipid bilayers of liposomes was less 15% (SSD/total lipid, molar ratio). Therefore, in DPPC/SSD (10:2)-liposome suspension, free SSD surely existed and would form micelles after bath sonication, resulting in the second endotherm peak of 40.38 °C. The value was similar to 40.12 °C in the endotherm of SSD suspension (Fig. 2), confirming that the endotherm of 40.38 °C in DPPC/SSD (10:2)-liposome suspension was the micelles of free SSD. But the endotherm of SSD suspension was broad as compared to the sharp endotherm of 40.38 °C in DPPC/SSD (10:2)-liposome suspension, a reason may

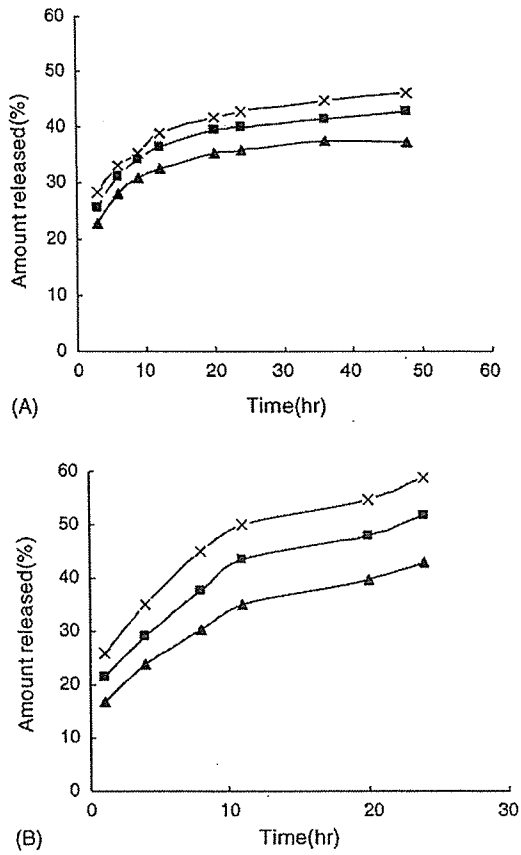

Fig. 3. Calcein release from liposomes at 37 ± 0.5 °C incubated with 1/10 PBS (A) and 30% rabbit plasma (B). (The data are means of two experiments.) (×): DPPC-liposomes, (■): DPPC/CHOL (10:4)-liposomes, (▲): DPPC/CHEMS (10:4)-liposomes.

be surmised that excessive SSD sedimentation might deposit on the base of aluminum pan, which may have interfered the heat conduction and subsequent peak appearance.

3.2. Calcein release study

Calcein release in 1/10 PBS (Fig. 3A) and in 30% rabbit plasma (Fig. 3B) were in duplicate since the experiments were parallel and the variability was very small. The results showed that the release of calcein from DPPC/CHEMS (10:4)-liposomes was slower than that of DPPC/CHOL (10:4)-liposomes, and the release in 1/10 PBS (Fig. 3A) was slower than that in 30% rabbit plasma (Fig. 3B).

3.3. Effect of CHEMS, CHOL and SSD on DPPC by FT-IR

The FT-IR spectrograms of DPPC/CHOL (1:1), DPPC/CHEMS (1:1) and DPPC/SSD (1:1) mixtures were compared with that of DPPC (Fig. 4).

Although the magnitude of the red shift is relatively small compared to the peak width (Asada et al., 2004), addition of CHOL, CHEMS and SSD in DPPC substantially induced the red shift of V_s P=O (from 1247.78 to 1241.99, 1240.07, 1235.21 cm^{-1}, respectively) and V_{as} P=O (from 1469.56 to 1465.71, 1467.64, 1465.71 cm^{-1}, respectively). We know that the asymmetry flexual vibration of the quaternary ammonium of DPPC is a small or side peak at 1670–1640 cm^{-1} (Peng, 1998). We can read from Fig. 4 that CHOL and SSD did not conceal the peak as there is no static electronic interaction between the hydroxyl groups and the quaternary ammonium of DPPC. While in the FT-IR spectrogram of the DPPC/CHEMS (1:1) mixture, the small peak (at 1670–1640 cm^{-1}) was absent, suggesting electrostatic interaction between the carboxyl group of CHEMS and the quaternary ammonium of DPPC.

3.4. SSD complex with CHOL but not with CHEMS

If SSD interacts with CHOL or CHEMS, it will insert lipid bilayers and ultimately disrupt the membrane structure of DPPC/CHOL (10:4)- or DPPC/CHEMS (10:4)-liposomes, causing large lipid aggregates to form and increasing the sedimentation and clarity of the supernatant of the liposome suspension.

To exclude an increase in clarity caused by liposome aggregation and sedimentation, distilled water was added. The results (Fig. 5) indicated there was no change in turbidity, which meant DPPC/CHOL (10:4)- and DPPC/CHEMS (10:4)-liposomes did not undergo sedimentation during the period of the experiment. After addition of SSD to DPPC/CHOL (10:4)- or DPPC/CHEMS (10:4)-liposomes, there was significant sedimentation for DPPC/CHOL (10:4)-liposomes and no turbidity change was observed for DPPC/CHEMS (10:4)-liposomes, which meant that SSD did not interact with CHEMS (Fig. 5).

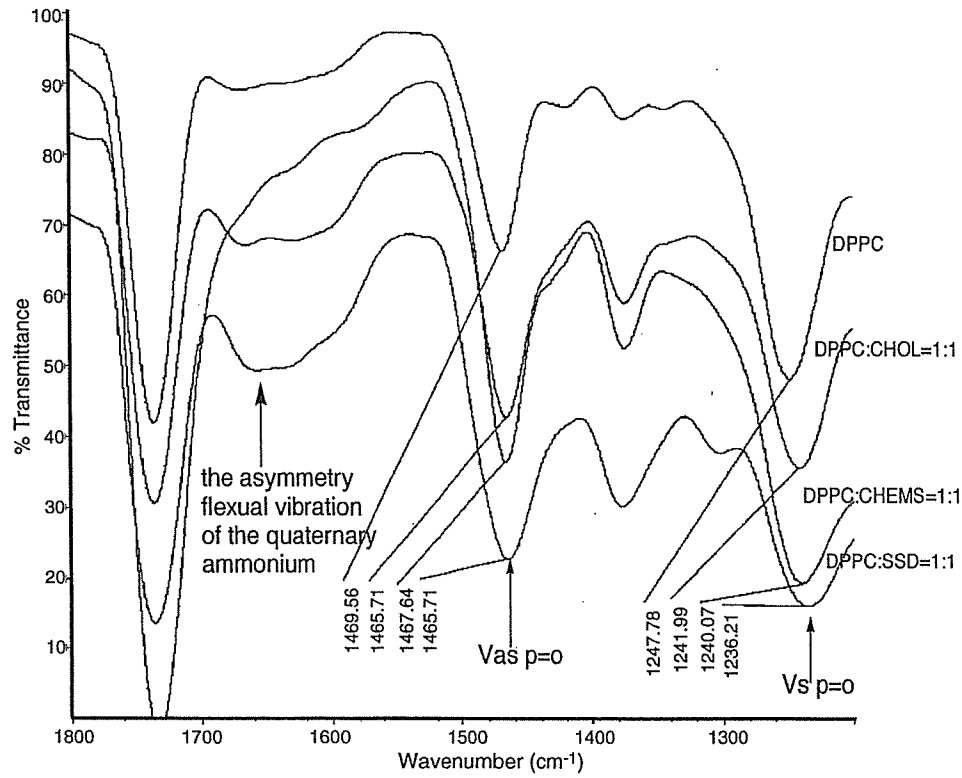

Fig. 4. FT-IR combinational spectrograms of DPPC mixtures with CHOL, CHEMS and SSD (1:1, molar ratio) between 1800 and 1200 cm^{-1}.

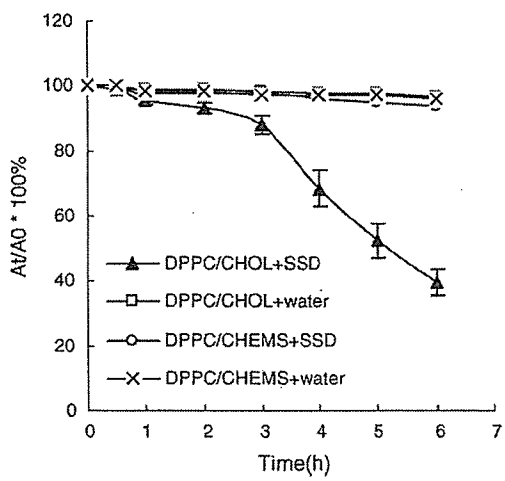

Fig. 5. Relative turbidity curve of DPPC/CHEMS (10:4)- and DPPC/CHOL (10:4)-liposomes (with a DPPC concentration of 0.5 mg/ml) after adding 200 μg/ml SSD suspension or distilled water. (The data are presented as mean ± S.D., $n = 3$.)

3.5. Hemolytic curve of SSD-liposomes

It seemed that DPPC/CHEMS/SSD (10:4:1)-liposomes could reduce the hemolytic activity of SSD in contrast to the SSD solution or the liposomes without CHEMS (DPPC/SSD (10:1)-liposomes) (Fig. 6). The liposomes that incorporated DSPE-PEG (DPPC/CHEMS/DSPE-PEG/SSD (10:4:0.5:1)-liposomes) showed the greatest ability to reduce the hemolytic activity. Thus, the SSD-liposomes should contain DSPE-PEG.

4. Discussion

In the present study, a value of the maximal transition temperature of 39.52 °C was observed for DPPC (Fig. 2), while a more usual literature value of 41 °C was reported. The great difference may be attributed to different lipid concentration used, different running conditions and different machines. We have found that

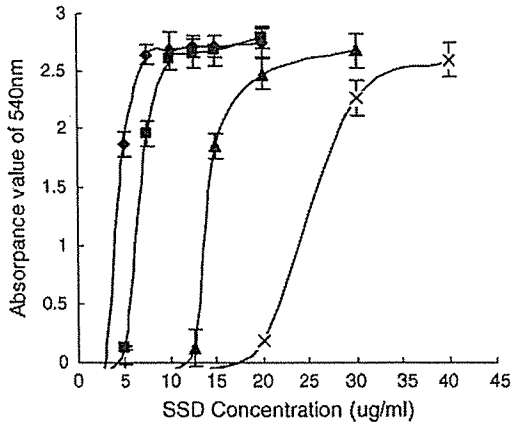

Fig. 6. Hemolytic curve of SSD solution and SSD-liposomes (with a lipid concentration of 2.5 mg/ml) on rabbit erythrocyte in vitro. (The data are presented as mean ± S.D., $n=3$.) (♦): SSD solution, (■): DPPC/SSD (10:1)-liposomes, (▲): DPPC/CHEMS/SSD (10:4:1)-liposomes, (×): DPPC/CHEMS/DSPE-PEG/SSD (10:4:0.5:1)-liposomes.

a less concentrated liposome suspension of 20 mg/ml of DPPC (10 μl equal to 0.2 mg of DPPC) produced a phase transition temperature of 40.5 °C, which is similar to the literature value. But, lower concentration of DPPC resulted in lower enthalpy value and lower sensitivity, therefore, 100 mg/ml of DPPC were employed during the experiments and the results allowed meaningful comparison since the experimental conditions were strictly controlled as the same for each other.

Addition of CHOL, CHEMS and SSD to DPPC-liposomes decreased the T_m and ΔH values of DPPC (Fig. 2 and Table 1), which accorded with the finding that introduction of a hydrophobic molecular within the lipid bilayers produces a decrease in T_m and ΔH (Mabrey and Sturtevant, 1976). As mentioned in the literature (Yang and Su, 1998; Wang, 1997), when above the phase transition temperature, the membrane fluidity drops when the area of the endothermic peak (ΔH value) decreases and the T_m value increases. Since the ΔH is markedly decreased as compared with the T_m, the reduction of ΔH is much more dominant while the decrease in T_m is negligible in membrane stabilization.

CHEMS could reduce the fluidity of the liposomal membrane according to the ΔH reduction (1.16 J/g for DPPC/CHEMS (10:1)-liposomes compared to 5.26 J/g for DPPC/CHOL (10:1)-liposomes), suggesting that CHEMS possesses more stabilization ability than CHOL. The result was supported by the calcein release study.

The hydroxyl group of CHOL and the sugar moiety of SSD can both form a hydrogen bond with the P=O bond of DPPC (Peng, 1998; Shimizu et al., 1996), which caused the red shift of V_s P=O and V_{as} P=O (Fig. 4). As for CHEMS, the red shift of V_s P=O and V_{as} P=O may be due to the fact that the carbonyl group of CHEMS can form a hydrogen bond with the P–OH bond of DPPC, and therefore affect the vibration of the P=O bond.

CHOL and CHEMS had a similar effect on the red shift of V_s P=O, while SSD had the strongest effect on the red shift of V_s P=O due to abundant hydroxyl groups on the sugar moiety of SSD. But maybe because of the small molecular volume of the hydroxyl group and succinic acid, together with the deep-anchored sterol ring reducing the hydrocarbon movement (Massey, 1998), they may fill the polar headspace of lipid bilayers and thus increase the membrane stability. As for SSD, although it had the strongest hydrogen interaction with the polar head of DPPC, it may disrupt the lipid arrangement due to the large molecular volume of the sugar moiety (Muramatsu et al., 1999), thus increasing the membrane fluidity.

Fig. 7 illustrates the proposed mechanism of interaction mechanism of DPPC with CHOL, CHEMS and SSD. The hydroxyl group of CHOL and the sugar moiety of SSD could form a hydrogen bond with the phosphorus oxygen double bond (P=O) of DPPC, then the electron cloud around the oxygen of P=O will migrate to the hydroxyl group, decreasing the polarity of P=O bond, and causing the red shift of the stretching vibration of P=O.

As for CHEMS, the carbonyl group of CHEMS might have hydrogen bond interaction with the P–OH bond of DPPC, then the electron cloud around the hydroxyl group of P–OH might become much more intense, and the increased electron cloud around the hydroxyl group of P–OH will migrate to the phosphorus atom of P–OH. Therefore, the decrease in the polarity of the P=O bond may cause a red shift. In addition, electrostatic interaction may exist between the carboxyl group of CHEMS and the quaternary ammonium of DPPC.

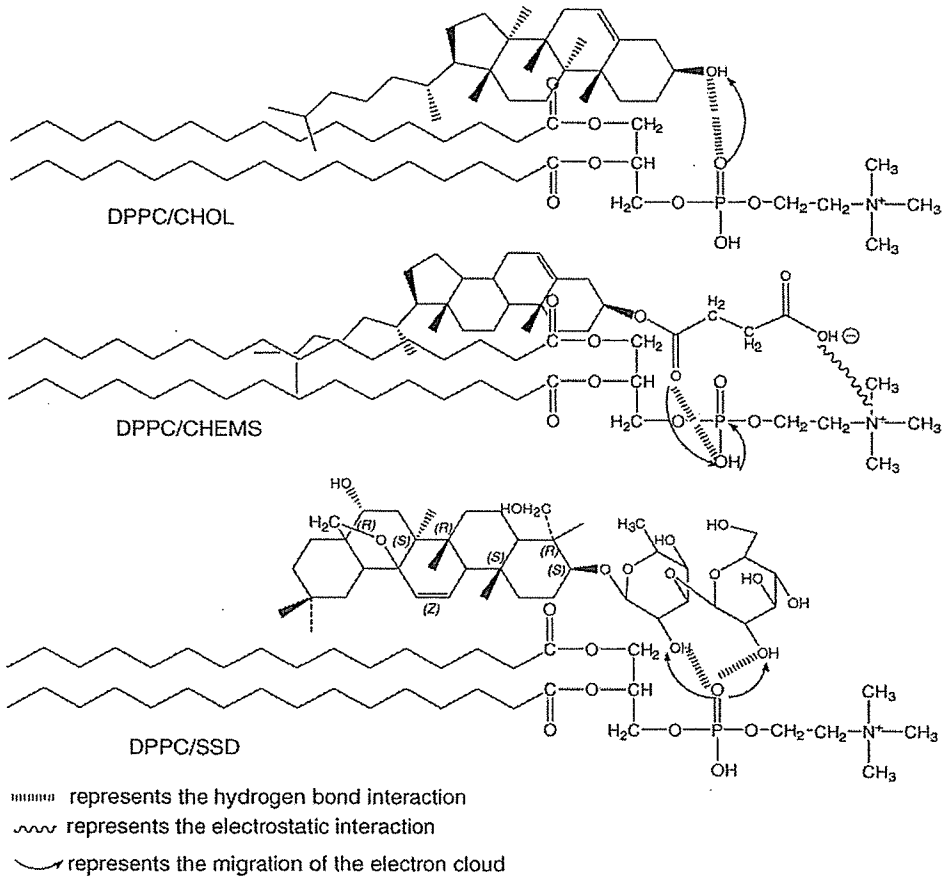

Fig. 7. Schematic diagram of interaction of DPPC with CHOL, CHEMS and SSD.

CHEMS can possess both hydrogen bond interaction and electrostatic interaction with DPPC membrane while CHOL only has hydrogen bond interaction. This difference may make the membrane of DPPC/CHEMS-liposomes more compact and steady than that of DPPC/CHOL-liposomes, being supported by the reduction of ΔH in DSC and low calcein release. In contrast, Massey (1998) reported that CHEMS could extend across one monolayer of the bilayer and partially interdigitate into the opposing monolayer of the bilayer, resulting in less membrane stabilization than CHOL by fluorescence polarization. From our study we hypothesized that the whole succinic group of CHEMS might fit into the polar head of DPPC and the sterol ring might be in the same position as that of CHOL.

CHEMS turned out to be a unique membrane stabilizer in SSD-liposomes due not to interaction with SSD as illustrated in Fig. 5. The reason may be ascribed to the succination of the hydroxyl group of CHOL, blocking recognition by SSD.

Further, CHEMS will find great use in the preparation of liposomes containing cholesterol-dependent hemolytic saponins. The incorporation of SSD into liposomes contained CHEMS could reduce its hemolytic activity (Fig. 6), because: SSD was incorporated in the lipid bilayers of liposomes, and liposomes containing CHEMS were negatively charged due to the presence of carboxylic acid residue and would experience repulsive interactions with erythrocyte membranes. In addition, reduced hemolytic activity of SSD-liposomes was observed on adding DSPE-PEG,

which may further exert a steric hindrance between liposome membranes and erythrocyte membranes.

This study has shown that CHEMS was more effective than CHOL in increasing DPPC membrane stability since CHEMS may possess both hydrogen bond interaction and electrostatic interaction with DPPC membrane while CHOL only has hydrogen bond interaction. Furthermore, CHEMS can be used as a unique membrane stabilizer in liposomes containing SSD. SSD-liposomes contained CHEMS and DSPE-PEG could greatly decrease the hemolytic activity of SSD.

Acknowledgment

This research was supported by a grant (30271520) from the National Science Foundation of China.

References

Abe, H., Orita, M., Konishi, H., Arichi, S., Odashima, S., 1986. Effects of saikosaponin-d on aminonucleoside nephrosis in rats. Eur. J. Pharmacol. 120, 171–178.

Asada, M., Takahashi, H., Okamoto, H., Tanino, H., Danjo, K., 2004. Theophylline particle design using chitosan by the spray drying. Int. J. Pharm. 270, 167–174.

Cheng, H.F., 1994. Saikasaponins for the treatment of nephritis. World Pharm. Newslett. 12, 24–25.

Cheng, S., Peng, C.E., Yang, M.J., 1999. The experimental research of Saikasaponins on the proliferation and matrix synthesis of hepatocyte. Chin. J. Basic Med. Tradit. Chin. Med. 28, 21–25.

Dumas, D., Muller, S., Gouin, S.F., Baros, F., Viriot, M.L., Stoltz, J.F., 1997. Membrane fluidity and oxygen diffusion in cholesterol-enriched erythrocyte membrane. Arch. Biochem. Biophys. 341, 34–39.

Fariss, M.W., Bryson, K.F., Hylton, E.E., Lippman, H.R., Stubin, C.H., Zhao, X.G., 1993. Protection against carbon tetrachloride-induced hepatotoxicity by pretreating rats with the hemisuccinate esters of tocopherol and cholesterol. Environ. Health Perspect. 101, 528–536.

Gregoriads, G., 1988. Liposomes as Drug Carriers: Recent Trends and Progress. Wiley, New York.

Ismail, M., Hafez, P., Cullis, R., 2000. Cholesteryl hemisuccinate exhibits pH sensitive polymorphic phase behavior. Biochim. Biophy. Acta 1463, 107–114.

Kida, H., Akao, T., Meselhy, M.R., Hattori, M., 1998. Metabolism and pharmacokinetics of orally administered saikosaponin b1 in conventional, germ-free and *Eubacterium* sp. A-44-infected gnotobiote rats. Biol. Pharm. Bull. 21, 588–593.

Kuhn, R.W., Schrader, W.T., Smith, R.G., O'Malley, B.W., 1975. Progesterone binding components of chick oviduct. J. Biol. Chem. 250, 4220–4228.

Lai, M.Z., Duzgunes, N., Szoka, F.C., 1985. Effects of the replacement of the hydroxyl group of cholesterol and tocopherol on the thermotropic behavior of phospholipid membranes. Biochemistry 24, 1646–1653.

Mabrey, S., Sturtevant, J.M., 1976. Investigation of phase transitions of lipids and lipid mixtures by high sensivity differential scanning calorimetry. Proc. Natl. Acad. Sci. U.S.A. 73, 3862–3866.

Massey, J.B., 1998. Effect of cholesteryl hemisuccinate on the interfacial properties of phosphatidylcholine bilayers. Biochim. Biophy. Acta 1415, 193–204.

Muramatsu, K., Takayama, K., Maitani, Y., 1999. The relationship between the rigidity of the liposomal membrane and the absorption of insulin after nasal administration of liposomes modified with an enhancer insulin in rabbit. Drug Dev. Ind. Pharm. 25, 1099–1105.

Nakamura, T., Kuriyama, M., Kosuge, E., 1993. Effect of saikosaponin on the production of platelet activating factor in human neutrophils. Ann. N.Y. Acad. Sci. 685, 572–579.

Peng, S.Q., 1998. Spectrogram Analysis of Drugs. Beijing Medical University Publishing House, Beijing, China, pp. 106–113.

Ray, S.D., Mumaw, V.R., Raje, R.R., Fariss, M.W., 1996. Protection of acetaminophen induced hepatocellular apoptosis and necrosis by cholesteryl hemisuccinate pretreatment. J. Pharmacol. Exp. Ther. 279, 1470–1483.

Se'rgio, S., Moreira, J.N., Cristina, F., 2004. On the formulation of pH-sensitive liposomes with long circulation times. Adv. Drug Delivery Rev. 56, 947–965.

Shimizu, K., Maitani, Y., Takayama, K., Nagai, T., 1996. Characterization of dipalmitoylphosphatidylcholine liposomes containing a soybean derived sterylglucoside mixture by differential scanning calorimetry, fourier transform infrared spectroscopy and enzymatic assay. J. Pharm. Sci. 85, 741–744.

Skornick, Y.G., Rong, G.H., Sindelar, W.F., Richert, L., Klausner, J.M., Rozin, R.R., Shinitzky, M., 1986. Active immunotherapy of human solid tumor with autologous cells treated with cholesteryl hemisuccinate. A phase I study. Cancer 58, 650–654.

Szoka, F., Papahadjopoulos, D., 1978. Procedure for preparation of liposomes with large internal aqueous space and high capture by reverse-phase evaporation. Proc. Natl. Acad. Sci. U.S.A. 75, 4194–4198.

Ushio, Y., Abe, H., 1991. Effect of saikosaponin-d on the function and morphology of macrophages. Int. J. Immunopharmacol. 13, 493–499.

Wang, B., 1997. The effect of cholesterol on the biomembrane fluidity. Acta Acad. Med. Guangxi 14, 34–36.

Wang, X.K., 1992. Tian Rang Yao Wu Hua Xue. People's Medical Publishing House, Beijing, China, pp. 524–541.

Wen, X.G., 1993. The transformation of Saikasaponin in xiong dan fu gan ning. Zhong ChengYao 3, 16–18.

Yang, L., Su, W.A., 1998. DSC, ESR and FP for the fluidity of membrane lipids. Acta Univ. Agric. Boreali-occidentalis 26, 99–104.

Yokoyama, H., Hiai, S., Oura, H., 1984. Effect of saikosaponins on dexamethasone suppression of the pituitary–adrenocortical system. Chem. Pharm. Bull. 32, 1224–1227.

Zhang, G.J., Liu, H.W., Yang, L., Zhong, Y.G., Zheng, Y.Z., 2000. Influence of membrane physical state on the lysosomal proton permeability. J. Membr. Biol. 175, 53–62.

Zhang, T.G., 1993. The study of Japanese Bupleurum formulation on the treatment of nephritis. Chin. J. Chin. Mater. Med. 18, 753–756.

Zhong, G.Y., Xue, K.X., Yuan, Y.W., Yan, J.S., 1993. Zhong Yao Zhi, 2nd ed. People's Medical Publishing House, Beijing, China, pp. 486.

Zhou, Q.L., Zhang, Z.Q., Nagasawa, T., Hiai, S., 1996. The structure activity relationship of saikosaponins and glycyrrhizin derivatives for Na^+, K^+-ATPase inhibiting action. Acta Pharm. Sin. 31, 496–501.

Available online at www.sciencedirect.com

SCIENCE DIRECT

Journal of Controlled Release 104 (2005) 313–321

journal of controlled release

www.elsevier.com/locate/jconrel

Influence of serum and albumins from different species on stability of camptothecin-loaded micelles

Praneet Opanasopit[a], Masayuki Yokoyama[b,*], Masato Watanabe[c], Kumi Kawano[c], Yoshie Maitani[c], Teruo Okano[a]

[a]*Institute of Advanced Biomedical Engineering and Science, Tokyo Women's Medical University, Kawada-cho 8-1, Shinjuku-ku, Tokyo 162-8666, Japan*

[b]*Kanagawa Academy of Science and Technology, KSP Bldg. East 404, Sakado 3-2-1, Takatsu-ku, Kawasaki-shi, Kanagawa-ken, 213-0012, Japan*

[c]*Institute of Medical Chemistry, Hoshi University, Ebara 2-4-41, Shinagawa-ku, Tokyo 142-8501, Japan*

Received 10 August 2004; accepted 18 February 2005
Available online 9 April 2005

Abstract

Stability of CPT free drug and CPT-loaded polymeric micelles forming from poly (ethylene glycol)-poly (benzyl aspartate-69) block copolymer in the presence of serum and purified serum albumins were investigated by reverse-phase HPLC and GPC. The hydrolysis of CPT and CPT-loaded micelles follows pseudo-first-order kinetics. The observed hydrolysis rate constants for CPT and CPT-loaded micelles were 7.4×10^{-3} min^{-1} and 0.7×10^{-3} h^{-1}, corresponding to an increase in half-life of CPT from 94 min to 990 h, respectively. The half-lives of CPT lactone hydrolysis of CPT-loaded micelles in the presence of BSA were significantly longer than the control whereas in the presence of HSA and serum was shorter than the control, and the similar results were obtained from GPC analyzed for micelles stability. This result suggested that the stability of CPT-loaded micelles was significantly decreased only in the presence of human albumin and serum. These were corresponded to the results of CPT free drug observed in the presence of albumins or serum. BSA significantly retarded the CPT lactone ring opening as compared with the control. On the other hand, HSA and serum showed rapid CPT lactone ring opening. This was probably due to preferential HSA binding to the carboxylate form resulting in a change in the lactone–carboxylate equilibrium, whereas, BSA did not bind to the lactone form, but might promote the self-aggregation of CPT and binding to the hydrophobic inner core of the micelles, resulting in enhanced stability of CPT-loaded micelles. MSA did not affect the stability of micelles.

Keywords: Serum; Albumin; Polymeric micelles; Camptothecin; Stability

* Corresponding author. Tel.: +81 44 819 2093; fax: +81 44 819 2095.
E-mail addresses: masajun@ksp.or.jp (M. Yokoyama), tokano@abmes.twmu.ac.jp (T. Okano).

0168-3659/$ - see front matter © 2005 Elsevier B.V. All rights reserved.
doi:10.1016/j.jconrel.2005.02.014

1. Introduction

A major problem currently associated with systemic drug administration is its even biodistribution throughout the body, resulting in the lack of specificity in its pharmacological activity to target cells. In addition, to reach the site of action drug has to overcome several biological barriers by which it may be inactivated. Camptothecin (CPT) is a potent, anticancer agent acting through the inhibition of topoisomerase I during the S-phase of the cell cycle [1]. It exists in two forms depending on the pH value, namely, an active lactone form at pH below 5 and an inactive carboxylate form at basic pH (Fig. 1a) [2]. At physiological pH, most CPT molecules exist in the inactive carboxylate form. The stable lactone form of CPT is critical for its anticancer activity. In addition, the ring opening carboxylate form shows poorer diffusibility through the lipid bilayer than the lactone form. Therefore, factors influencing a lactone–carboxylate equilibrium within the CPT molecule are clearly important determinants of the agent's function. Human serum albumin (HSA) was shown to bind preferentially with the carboxylate form, resulting in the lactone ring opening more rapidly [3,4]. However, serum albumins from other species were found to bind CPT carboxylate not as tightly as HSA [5]. In addition, Nabiev et al. [6,7] reported that BSA did not participate in binding of the lactone, carboxylate, or self-aggregate of CPT. This fact may result in differences between clinical trials and animal experiments of this drug. Red blood cells stabilize the biologically active form of CPT by allowing the lactone ring to partition into lipid bilayers, thereby protecting the moiety from hydrolysis [3]. Nabiev et al. [6,7] discovered a novel effect certainly influencing the biological activity of CPT: at low concentrations in aqueous buffer solutions, stable J-type aggregates formed by the stacking interaction between the quinoline rings of the CPT chromophores with the inverse position of the nitrogen atoms. This self-aggregation partially prevents hydrolysis of the lactone ring at neutral pH values and J-aggregates were found to penetrate within the cells with much higher efficiency than the monomers of the drug.

A number of delivery systems are under development for targeted and controlled delivery of drugs. When entering into the systemic circulation by intravascular administration or through absorption at the administration site, a delivery system carrying pharmaceuticals encounters blood cells and plasma proteins before reaching its target cells. Serum proteins, erythrocytes and other blood cells can bind to the drug carriers leading to an alteration in its physicochemical properties such as particle size and electrical charge [8]. If it interacts with those blood components,

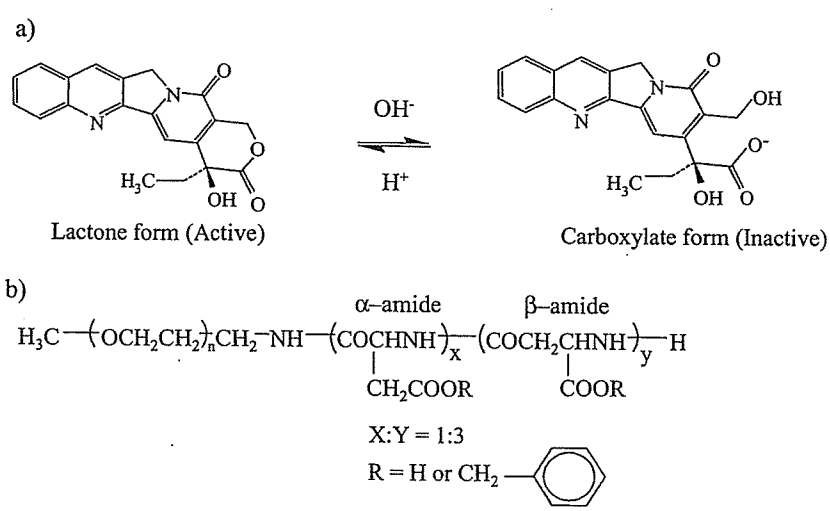

Fig. 1. (a) Chemical structure of camptothecin (CPT) two forms depending on the pH value, namely, an active lactone form at pH below 5 and an inactive carboxylate form at basic pH. (b) Chemical structure of poly(ethylenglycol)-poly(benzyl aspartate 69) block copolymers.